Structural investigation of flat overlayer and surface alloy of Sn on Mo(110)

Chen, Xiaobin
Department of Molecular and Material Sciences, Interdisciplinary Graduate School of Engineering Sciences, Kyushu University

Banik, Dhiman
Department of Molecular and Material Sciences, Interdisciplinary Graduate School of Engineering Sciences, Kyushu University

Nakagawa, Takeshi
Department of Molecular and Material Sciences, Interdisciplinary Graduate School of Engineering Sciences, Kyushu University

出版情報：Surface Science. 729, pp.122224-, 2023-03. Elsevier
バージョン：
権利関係：

Structural investigation of flat overlayer and surface alloy of Sn on Mo(110)

Xiaobin Chen[1], Dhiman Banik[1], and Takeshi Nakagawa[1, 2, *]

[1]*Department of Molecular and Material Sciences, Interdisciplinary Graduate School of Engineering Sciences, Kyushu University, 6-1 Kasuga Koen, Kasuga, Fukuoka 816-8580, Japan*

[2]*Department of Advanced Materials Science and Engineering, Faculty of Engineering Sciences, Kyushu University, 6-1 Kasuga Koen, Kasuga, Fukuoka 816-8580, Japan*

*corresponding author: nakagawa.takeshi.174@m.kyushu-u.ac.jp

Abstract

Atomic structures of Sn on Mo(110) are investigated using low-energy electron diffraction (LEED) and density functional theory (DFT) calculation. Sn atoms occupy substitutional sites at elevated temperatures in (3×1) structure, corresponding to a coverage of 0.33 ML. The substitutional model agrees with previous LEED, workfunction, and STM results after annealing to 800 K. For (1×3) structure at 0.67ML, Sn atoms adsorb in the nearest three-fold hollow sites. With increasing Sn coverage, the (1×4) structure at 0.75ML, Sn atoms start to fill four-fold hollow sites. On both overlayer phases, Sn structures are flat without significant buckling. Compared with a two-dimensional tin, stanene, which is a stacking of α-Sn(111), Sn overlayer on Mo(110) is not related to α-Sn(111) but to β-Sn(100), which is normal metallic.

Keywords

Sn; Mo(110); LEED; DFT; Surface atomic structure; Surface alloy

1. Introduction

The growth of Sn films has attracted interest due to the advent of two-dimensional atomic layers. Stanene, a two-dimensional Sn layer, is a candidate for a 2D topological insulator. The bulk band gap of stanene can be so large, 0.3 eV, that is enough for practical applications at room temperature [1]. After the first successful growth of monolayer stanene on a Bi_2Te_3(111) [2], stanene has been epitaxially grown on Sb(111), InSb(111) , Au(111), Ag(111), Cu(111), PbTe(111) and other substrates [3–8] .

On the other hand, Mo is often used to study the growth of metals due to its high thermal stability and low reactivity against to metals, offering detailed insights into the energetic and geometric interactions between surfaces and adsorbates. Plenty of surface structures and growth modes have been investigated on Mo(110) in several works such as Sn[9–11], Pb[12–14], In[15]. However, the adsorption of Sn on Mo has not been sufficiently studied, and its basic properties, such as adsorption

structure, are not fully understood. It is, therefore, necessary to clarify the detailed adsorption structure to understand the interaction and reaction of Sn on the Mo(110) surface.

The deposition of Sn on Mo has been studied extensively by Tikhov *et al.* [11] using low-energy electron diffraction (LEED), Auger electron spectroscopy (AES), workfunction measurements, and thermal-desorption spectroscopy (TDS). The (1×3) and (1×4) LEED patterns at coverages of about 0.67 and 0.75 ML had been reported at room temperature. (3×1) at 0.33ML and other LEED patterns at high temperatures or after annealing were also observed. They proposed a corresponding structure model for annealed low coverage (3×1) structure (they described (3×1) as (3×2)). It appears appropriate to incorporate all Sn in the (3×1) structure into the topmost layer to form a surface alloy. Even though there is no detailed structural model for (1×3) and (1×4) structure in Sn/Mo system, there are few suggestions available concerning similar systems Pb/Mo (110)[10], Sn/W(110)[16] and In/W(110)[17]. For (1×3) structure, all Pb atoms are aligned in the substrate $[1\bar{1}1]$ directions, which is the most closely packed substrate direction. In the case of Sn/Mo(110), Sn atoms were assumed to adsorb on the most energetically favorable four-fold hollow sites, gradually filling three-fold hollow sites or short bridge sites for both (1×3) and (1×4) structures. For (1×4) structure in In/W(110) [17], Stöhr *et al.* reported that In adsorption in fourfold hollow sites is preferable since the adsorption energy is minimum and that adsorption of the In atoms in the pseudo-threefold site provides a reasonable compromise between optimum chemical adsorption and large stress within the In adlayer. Therefore, the overall bonding is strengthened. Scanning tunneling microscopy (STM) and AES reveals that the growth behavior of thin Sn films on the Mo (110) surface at room temperature is layer-by-layer for the first two layers of Sn [8]. At elevated temperatures at ~ 800 K, STM measurement observed the rearrangement of film, suggesting a Sn–Mo surface alloy formation. Despite these elaborated works, structural determination of submonolayer Sn on Mo(110) has not been attempted, and the relevance to allotropes of Sn remains unknown.

In this work, we determined the submonolayer structures of Sn adsorption on Mo(110) using dynamical LEED analysis combined with *ab* initio density functional theory (DFT) calculations. The low coverage structure of 3×1, formed upon annealing, is surface alloy, while the high coverage structures, 1×3 and 1×4, show overlayer structure. The densest overlayer structure, 1×4, is similar to the β-Sn(white Sn), indicating that monolayer Sn on Mo(110) is metallic.

2. Experimental

Experiments were performed in an ultrahigh vacuum chamber equipped with a four-grid LEED system, including *in-situ* sample preparation and Sn evaporator. The base pressure of the chamber was lower than 5×10^{-8} Pa. Sn thin films were evaporated by thermal heating from a tantalum tube onto the Mo (110) substrate. Mo(110) was cleaned by repeated cycles of oxidation with the oxygen pressure of 5×10^{-6} Pa at ~1500 K for 10 mins and subsequent flashing at 2100 K for 10 s until a sharp (1×1) LEED pattern was obtained.

Successive LEED patterns as a function of an acceleration voltage of incident electrons were recorded at T_s = 120 K using a CCD camera from 80 to 500 eV with a step of 1 eV. LEED *I–V* curves were extracted from the LEED patterns and compared with a dynamical LEED calculation. The Barbieri/Van Hove symmetrized automated-tensor LEED package was used to calculate the theoretical curves [18]. Structural optimization was performed based on the Pendry reliable factor (R_P) by comparing experimental and theoretical curves [19]. The error limits of the structural parameters were estimated from the variance of the R_P, $\Delta R_P = R_{min}\,(8V_{0i}/E_t)^{1/2}$, where R_{min}, E_t, and V_{0i} are the minimum of R_P, the total energy width, and the inner potential, respectively. The total energy widths for p(3×1), p(1×3), and p(1×4) surfaces were 4493, 2575, and 3107 eV, respectively. All the crystal structures were visualized using VESTA [20].

DFT calculations were performed to verify and analyze the experimental results using the Quantum Espresso package [21,22]. The exchange-correlation function was approximated within the generalized gradient approximation as parametrized by Perdew, Burke, and Ernzerhof (PBE) [23]. In all calculations, the chosen energy cutoff for the plane wave and for the charge density were 600 eV and 5100 eV, respectively, and the threshold for self-consistency was 1×10^{-6} eV. The Brillouin-zone integration was performed using a Monkhorst-Pack k-point sampling [24], with a 12×12×1 k-point mesh for the 1×1 (110) surface, and for larger unit cells, the meshes were scaled accordingly.

The symmetric surface slab was modeled with seven layers of Mo and Sn atoms on both sides. A region of approximately 10 Å of vacuum was inserted to prevent interactions between the slabs. The middle Mo layer was kept fixed during the geometry relaxation, and the positions of all the other atoms were optimized until two conditions were simultaneously satisfied: the forces on each atom were less than 0.03 eV/Å, and the energy difference of consecutive steps was less than 0.01 eV.

3. Results and discussion

3.1 DFT evaluation of adsorption energy of single Sn adsorption

In order to analyze the interaction of Mo(110) substrate with a single Sn atom, we calculated adsorption energies, E_{ads}, per Sn adatom for a (4×4) unit cell. We obtained the adsorption energy for substitutional as well as overlayer adsorption using the following equations:

$$E_{ads}(\text{overlayer}) = -1/n(E_{\text{Sn/Mo(110)}} - E_{\text{Mo(110)}} - nE_{\text{Sn}})$$

$$E_{ads}(\text{substitutional}) = -1/n(E_{\text{Sn/Mo(110)}} - E_{\text{Mo(110)}} - nE_{\text{Sn}} + nE_{\text{Mo(bulk)}})$$

, where n is the number of Sn atoms in the unit cell, $E_{\text{Sn/Mo(110)}}$ is the energy of the superstructure, $E_{\text{Mo(110)}}$ is the energy of the corresponding clean Mo(110) slab, E_{Sn} is the energy of an isolated Sn atom, and $E_{\text{Mo(bulk)}}$ is the energy of the bulk Mo atom. We have calculated adsorption energy for five sites (four-fold hollow, three-fold hollow, short bridge, on-top and substitutional sites) as shown in Fig.1 (a).

Table 1 shows the adsorption energies for isolated Sn atoms. When we consider that the adsorbed atoms form a surface alloy with the substrate, the substitutional site shows the lowest E_{ads} values of -4.61 eV/atom. For an Sn overlayer on the Mo substrate, the four-fold hollow site is the most favorable (-4.22 eV), followed by the three-fold (-4.05 eV), short bridge (-3.84 eV), and on-top sites (-3.46 eV). These results are similar to In/W(110) [17] and Pb/Mo(110) [13] systems. M. Stöhr identified that the lateral forces drive the In atom toward the four-fold hollow site [17]. Therefore we could expect a similar explanation to follow in Sn/Mo(110) case.

3.2 Surface alloy formation at low Sn coverage

We prepared (3×1) structure with Sn deposition at 800 K as shown in Fig. 1(c). According to previous reports, the Sn coverage for (3×1) corresponds to 0.33ML. The (3×1) supercell is specified relative to the basis vectors $\boldsymbol{a_1}'$ in the direction of $[1\bar{1}1]$ and $\boldsymbol{a_2}'$ in the direction of $[1\bar{1}0]$. The reciprocal lattice vectors $\boldsymbol{b_1}'$ and $\boldsymbol{b_2}'$ correspond to the above basis vectors are shown in Fig.1(c), which is different from conventional reciprocal lattice vectors $\boldsymbol{b_1}$ and $\boldsymbol{b_2}$ for the clean Mo(110) surface.

Using LEED *I-V* analysis, we have determined the (3×1) structure. We constructed an atomic model of the (3×1) structure as an ordered alloyed layer with one Sn atom and two Mo atoms in the unit cell, as shown in Fig. 2(a). With LEED I-V analysis, the substitutional model shows fair agreement with the experimental results as shown in Fig. 3 (a), with the lowest R_p of 0.17. The overlayer model with Sn in the hollow sites does not reproduce the experimental results with R_p of 0.61. The substitutional sites in the first layer are preferred by Sn atoms, which form a surface alloy with Mo(110) instead of an overlayer. It is consistent with the previous report [11]. After annealing at 700 K – 900 K, LEED observation shows the (3×1) pattern, which accompanied a significant decrease of workfunction and surface dipole compared with the ones prepared at room temperature [11]. STM measurements after 800 K annealing also show a significant depression of overlayer Sn, suggesting alloy formation of Sn with Mo [8].

In order to certify the LEED results, we performed ab initio DFT calculations to evaluate the Sn adsorption energy for the two models using the following equations. DFT calculations show that the preferred adsorption site for (3×1) is the substitutional site with the adsorption energy of -4.72 eV, which is lower than -4.17 eV for hollow sites.

In Table.1, we show the experimental LEED and DFT structure parameters for (3×1) structure. The LEED and DFT results show a good agreement. The Sn atoms adsorb on the Mo(110) surface occupying substitutional sites, and the surface structure shows significant buckling and contraction. Sn is not coplanar with the first Mo layer but buckled above the Mo plane by 0.56 ± 0.02 Å and 0.65 Å according to LEED and DFT calculations. A 5.4% contraction of the surface layer spacing between the first and second Mo layers compensates for the valence electron depletion on the surface and reduces the surface stress.

When comparing the experimental and theoretical values of the distance between Sn atoms and nearest neighbor Mo atoms in surface alloys, the experimental distance (2.80 Å) is smaller than the theoretical sum of Sn and Mo radii (2.98 Å). The reduced distance is consistent with previous results

for surface alloys (Ni-Pb, Cu-Au, Cu-Sb, and Ag-Sb) [25]. The adsorbate–substrate distance in the surface alloy is significantly less than that calculated based on the sum of the atomic radii in the elemental solids. The reduction of the atomic distance on the surface has been attributed to the significant difference in the bonding at the surface, indicating that these surface alloys may have significant covalent properties.

The surface alloy model is consistent with the previous results based on the workfunction measurements [11]. Tikhov *et al.* suggested that the distorted $MoSn_3$(100) forms a coincidence lattice with Mo(110) with the (3×1) structure. The distortion gives an excellent fit to the substrate but requires a substantial compression of the $MoSn_3$ (100) plane [11].

In the case of Indium on W(110) and Sn on W (110) [16,17], (3×1) structure was also observed at room temperature, which is not the case for Sn/Mo(110). In/W(110) and Sn/W(110), the hollow sites are assumed to be preferred by adsorbates, creating an overlayer on the substrates. The overlayer model for (3×1) is different from our conclusion. On the other hand, the formation of (3×1) for Sn/Mo(110) occurs only at high temperatures (~ 800 K). It was suggested that the alloy formation on In/W(110) was improbable since larger activation energy of 5 eV was necessary. At a temperature approaching 800 K, however, the diffusion mean free path is long enough for Sn atoms to reach the step edges according to STM observation, and the exchange between Sn and Mo at step edges would be easier, resulting in the surface alloy formation.

3.3 Overlayer structures of 1×3 and 1×4 at high Sn coverage

With increased Sn deposition at room temperature, we observed a (1×3) pattern by LEED as shown in Fig. 1(d), which corresponds to Sn coverages of 0.67 ML[11]. The (1×3) supercell is specified relative to the base vectors $\boldsymbol{a_1}''$ in the direction of $[001]$ and $\boldsymbol{a_2}''$ in the direction of $[1\bar{1}1]$. Fig. 2(b) shows the optimized model, which gives the best R_p (0.24) obtained from the *I-V* LEED analysis as shown in Fig. 3(b). Two Sn atoms in the unit cell occupy the nearest three-fold hollow sites, not four-fold hollow sites. The DFT calculation also confirms that the adsorption energy of Sn under this model is the smallest (-4.37 eV).

It seems surprising that Sn does not adsorb on the most stable site for single Sn adsorption, the four-fold hollow site. The previous experiments assumed Sn adsorption at the four-fold site for 1×3 structure [11]. Two Sn atoms cannot occupy the four-fold hollow sites simultaneously due to size mismatch, which results in an elastic energy gain of +0.45 eV/atom compared with the optimized structure as revealed by DFT. Other possible configurations of two Sn atoms such as the four-fold and bridge (+0.16 eV/atom), the four-fold and three-fold (+0.11 eV/atom), are slightly unstable compared with the three-fold and three-fold case. Sn does not adsorb on the four-fold sites for 1×3 structure.

We summarize the structure parameter of the optimized (1×3) model in Table 2. Both *I-V* analysis and DFT give nearly identical results. Sn1 atoms locate 2.35 Å (DFT:2.44 Å) above the average Mo plane. Since all Sn atoms occupy three-fold sites, there is no buckling. The average distance between first and second Mo layer is 2.22 Å (DFT:2.23 Å), which is longer than 2.17 Å for clean Mo(110). The strong bonding could explain the increased Mo interlayer distance toward the Sn layer between Sn and

Mo. The second layer Mo hardly changes their position, which means Sn adsorption hardly affects the inner layer atoms and only has a strong bonding with the first layer atoms.

According to STM measurements, the first two layers of Sn grow layer by layer at room temperatures, and for submonolayer coverage, Sn atoms prefer to nucleate randomly [9]. Therefore, the model involving Sn atoms in the substitutional sites is less suitable. Although the four-fold hollow sites would be energetically preferable, the adsorption sites of one Sn in four-fold hollow sites and the other one in the three-fold, which is the model for Pb/Mo system [11], have not been applied to Sn/Mo(110). The lateral force between Sn atoms makes the distance of Sn rather uniform. The distances between next-neighbor three Sn atoms are 3.15 Å, 3.55 Å, and 3.48 Å along the direction $[001]$, $[1\bar{1}1]$ and $[1\bar{1}0]$, respectively.

We observed (1×4) LEED pattern as shown in Fig. 1(e), with increasing Sn coverage at room temperature, in agreement with the previous results [10,11]. The ideal coverage for 1×4 is 0.75 ML. Fig. 2(c) shows the optimized structure model for (1×4), which gives the best R_p (0.17) in LEED *I-V* analysis as shown in Fig. 3(c). In this optimized model, one Sn atom (Sn1) sits in the four-fold hollow sites, and the other two Sn atoms (Sn2, Sn3) occupy the nearest three-fold hollow sites. The adsorption position is not entirely four-fold hollow sites which is energetically the most favorable site. The combination of the adsorption sites is consistent with proposed models for (1×4) structures on In/W(110) [17] and Cl/Mo(110) [26]. In Cl/Mo(110), the atomic radius of Cl is so large (1.5 Å) that the Cl atoms in the cell are pushed from the four-fold hollow to the center of the unit cell. For In/W(110) M. Stöhr *et al*. suggested that adsorption of the In atoms in or close to the pseudo-threefold site provides a reasonable compromise between optimum chemical adsorption and considerable stress within the In adlayer [17]. In this work, however, Sn atoms first occupy three-fold hollow sites at the coverage of 0.67ML due to the lateral force from near Sn atoms, then start occupying four-fold hollow sites.

As Sn coverage increases, Sn atoms move toward the nearest stable sites. In addition, The DFT calculation results also confirm that the adsorption energy of Sn of the model is the lowest (-4.22 eV). In contrast to the adsorption energy of (1×3) structure (-4.37 eV), the average adsorption energy slightly decreases, even though Sn starts to occupy the favorable four-fold hollow site. The decreased adsorption energy with increasing Sn coverage indicates that the interaction between Sn atoms on Mo surface is repulsive [11].

Table 3 shows the structure parameters of (1×4). The parameters obtained from DFT reasonably agree with those from *I-V* analysis. Sn atoms at the four-fold hollow sites locate 2.44Å (DFT:2.50 Å) above the average Mo plane. In contrast, Sn atoms at the three-fold hollow sites lie in the lower position, 2.40 Å (DFT:2.44 Å) above the first Mo plane, causing slight buckling of 0.04 Å (DFT:0.06 Å). The average distance between the first and second Mo layer is 2.21 Å (DFT:2.20 Å), which is shorter than 2.22Å (DFT:2.23 Å) for (1×3) structure. Due to the denser Sn overlayer in the (1×4) structure, the Mo interlayer distance between the first and second layer decreases and shifts toward the bulk compared with (1×3) structure. As (1×3) structure, the rearrangement of Sn atoms in the surface layer makes the distance of Sn rather uniform. The distance between the nearest Sn atoms is 3.15 Å along $[001]$ and

$[1\bar{1}0]$, and 3.28 Å along $[1\bar{1}1]$, indicating a metallic bond. As shown in Figs. 2(b) and (c), all the Sn atoms in (1×3) are surrounded by five Sn atoms. In (1×4), Sn at the four-fold hollow site (Sn1) is surrounded by six Sn, while the ones at the three-fold hollow site (Sn2, Sn3) by five Sn.

The Sn forms dense and flat overlayers on Mo(110) at room temperatures and the (1×4) structure resembles β-Sn(100) closely as shown in Fig. S1 [27], which is a metal and the stable form of Sn at ambient conditions. The [001] direction of (1×4) is parallel to the [001] of β-Sn(100). On the other hand, stanene are considered as a stacking of α-Sn(111). The unit cell of β-Sn(100) is a rectangular of 3.17 Å × 5.82 Å and the atomic density is 1.07×10^{19} /m^2, which is close to that of 1×4 structure, 1.08×10^{19} /m^2. The structural analysis indicates that Sn overlayer on Mo(110) is metallic.

4. Conclusion

We have determined some ordered Sn structures on Mo(110) using LEED *I-V* analysis. Sn forms ordered surface alloy, 3×1 structure, for the coverage less than 1/3 ML upon annealing at 800 K, while it shows overlayer structures of (1×3) and (1×4) for the coverage more than 1/3 ML. From the DFT calculation, the four-fold hollow site is the most stable for a single Sn, followed by the three-fold hollow site. On the other hand, for the ordered structures, Sn atoms first adsorb in the three-fold hollow sites for (1×3) at 0.67ML. With increasing Sn coverages, Sn atoms start to fill the four-fold hollow sites after three-fold hollow sites and form (1×4) at 0.75ML. In the (1×4) structure, Sn atoms have a relatively uniform bond length between 3.15-3.28 Å, and the number of adjacent Sn atoms is five or six, depending on the adsorption sites. Compared with the bulk Sn structures, the 1×4 structure resembles β-Sn(100), indicating that the Sn overlayer on Mo(110) is of a metallic nature, not covalent.

Acknowledgments

This work was supported by JSPS KAKENHI Grant Number JP22K04928.

References

[1] Y. Xu, B. Yan, H.-J. Zhang, J. Wang, G. Xu, P. Tang, W. Duan, S.-C. Zhang, Large-Gap Quantum Spin Hall Insulators in Tin Films, Phys Rev Lett. 111 (2013) 136804. https://doi.org/10.1103/PhysRevLett.111.136804.

[2] F. Zhu, W. Chen, Y. Xu, C. Gao, D. Guan, C. Liu, D. Qian, S.-C. Zhang, J. Jia, Epitaxial growth of two-dimensional stanene, Nat Mater. 14 (2015) 1020–1025. https://doi.org/10.1038/nmat4384.

[3] J. Gou, L. Kong, H. Li, Q. Zhong, W. Li, P. Cheng, L. Chen, K. Wu, Strain-induced band engineering in monolayer stanene on Sb(111), Phys Rev Mater. 1 (2017) 054004. https://doi.org/10.1103/PhysRevMaterials.1.054004.

[4] C.-Z. Xu, Y.-H. Chan, P. Chen, X. Wang, D. Flötotto, J.A. Hlevyack, G. Bian, S.-K. Mo, M.-Y. Chou, T.-C. Chiang, Gapped electronic structure of epitaxial stanene on InSb(111), Phys Rev B. 97 (2018) 035122. https://doi.org/10.1103/PhysRevB.97.035122.

[5] M. Maniraj, B. Stadtmüller, D. Jungkenn, M. Düvel, S. Emmerich, W. Shi, J. Stöckl, L. Lyu, J. Kollamana, Z. Wei, A. Jurenkow, S. Jakobs, B. Yan, S. Steil, M. Cinchetti, S. Mathias, M. Aeschlimann, A case study for the formation of stanene on a metal surface, Commun Phys. 2 (2019) 12. https://doi.org/10.1038/s42005-019-0111-2.

[6] J. Yuhara, Y. Fujii, K. Nishino, N. Isobe, M. Nakatake, L. Xian, A. Rubio, G. le Lay, Large area planar stanene epitaxially grown on Ag(1 1 1), 2d Mater. 5 (2018) 025002. https://doi.org/10.1088/2053-1583/aa9ea0.

[7] Y. Zang, T. Jiang, Y. Gong, Z. Guan, C. Liu, M. Liao, K. Zhu, Z. Li, L. Wang, W. Li, C. Song, D. Zhang, Y. Xu, K. He, X. Ma, S. Zhang, Q. Xue, Realizing an Epitaxial Decorated Stanene with an Insulating Bandgap, Adv Funct Mater. 28 (2018) 1802723. https://doi.org/10.1002/adfm.201802723.

[8] R. Ahmed, T. Nakagawa, S. Mizuno, Structure determination of ultra-flat stanene on Cu(111) using low energy electron diffraction, Surf Sci. 691 (2020) 121498. https://doi.org/10.1016/J.SUSC.2019.121498.

[9] A. Krupski, Growth of Sn on Mo(110) studied by AES and STM, Surf Sci. 605 (2011) 1291–1297. https://doi.org/10.1016/j.susc.2011.04.020.

[10] Y. Maehara, T. Kimura, H. Kawanowa, Y. Gotoh, Surface structures of Sn on Mo(110) surface investigated by RHEED, J Cryst Growth. 275 (2005) e1619–e1624. https://doi.org/10.1016/j.jcrysgro.2004.11.201.

[11] M. Tikhov, E. Bauer, The interaction of Pb and Sn with the Mo(110) surface, Surf Sci. 203 (1988) 423–448. https://doi.org/10.1016/0039-6028(88)90092-1.

[12] A. Krupski, Pb on Mo(110) studied by scanning tunneling microscopy, Phys Rev B. 80 (2009) 035424. https://doi.org/10.1103/PhysRevB.80.035424.

[13] K. Kośmider, A. Krupski, P. Jelínek, L. Jurczyszyn, Atomic and electronic properties of the Pb/Mo(110) adsorption system, Phys Rev B. 80 (2009) 115424. https://doi.org/10.1103/PhysRevB.80.115424.

[14] S. Jo, Y. Gotoh, T. Nishi, D. Mori, T. Gonda, Surface structures of lead deposited on Mo(110) surface, Surf Sci. 454–456 (2000) 729–735. https://doi.org/10.1016/S0039-6028(00)00267-3.

[15] A. Katoh, H. Miwa, Y. Maehara, H. Kawanowa, Y. Gotoh, Studies on surface structures and growth of In ultrathin films on Mo(110) surface, Surf Sci. 566–568 (2004) 181–185. https://doi.org/10.1016/j.susc.2004.05.042.

[16] S. Chakraborty, K.S.R. Menon, Growth, structural evolution and electronic properties of ultrathin films of Sn on W(110), Surf Sci. 674 (2018) 79–86. https://doi.org/10.1016/j.susc.2018.04.004.

[17] M. Stöhr, R. Podloucky, M. Gabl, N. Memmel, E. Bertel, Combined ab initio and LEED I/V study of submonolayer adsorption of In on W(110), Phys Rev B. 76 (2007) 195449. https://doi.org/10.1103/PhysRevB.76.195449.

[18] M.A. van Hove, W. Moritz, H. Over, P.J. Rous, A. Wander, A. Barbieri, N. Materer, U. Starke, G.A. Somorjai, Automated determination of complex surface structures by LEED, Surf Sci Rep. 19 (1993) 191–229. https://doi.org/10.1016/0167-5729(93)90011-D.

[19] J.B. Pendry, Reliability factors for LEED calculations, Journal of Physics C: Solid State Physics. 13 (1980) 937–944. https://doi.org/10.1088/0022-3719/13/5/024.

[20] K. Momma, F. Izumi, VESTA 3 for three-dimensional visualization of crystal, volumetric and morphology data, J Appl Crystallogr. 44 (2011) 1272–1276. https://doi.org/10.1107/S0021889811038970.

[21] P. Giannozzi, S. Baroni, N. Bonini, M. Calandra, R. Car, C. Cavazzoni, D. Ceresoli, G.L. Chiarotti, M. Cococcioni, I. Dabo, A. Dal Corso, S. de Gironcoli, S. Fabris, G. Fratesi, R. Gebauer, U. Gerstmann, C. Gougoussis, A. Kokalj, M. Lazzeri, L. Martin-Samos, N. Marzari, F. Mauri, R. Mazzarello, S. Paolini, A. Pasquarello, L. Paulatto, C. Sbraccia, S. Scandolo, G. Sclauzero, A.P. Seitsonen, A. Smogunov, P. Umari, R.M. Wentzcovitch, QUANTUM ESPRESSO: a modular and open-source software project for quantum simulations of materials, Journal of Physics: Condensed Matter. 21 (2009) 395502. https://doi.org/10.1088/0953-8984/21/39/395502.

[22] P. Giannozzi, O. Andreussi, T. Brumme, O. Bunau, M. Buongiorno Nardelli, M. Calandra, R. Car, C. Cavazzoni, D. Ceresoli, M. Cococcioni, N. Colonna, I. Carnimeo, A. Dal Corso, S. de Gironcoli, P. Delugas, R.A. DiStasio, A. Ferretti, A. Floris, G. Fratesi, G. Fugallo, R. Gebauer, U. Gerstmann, F. Giustino, T. Gorni, J. Jia, M. Kawamura, H.-Y. Ko, A. Kokalj, E. Küçükbenli, M. Lazzeri, M. Marsili, N. Marzari, F. Mauri, N.L. Nguyen, H.-V. Nguyen, A. Otero-de-la-Roza, L. Paulatto, S. Poncé, D. Rocca, R. Sabatini, B. Santra, M. Schlipf, A.P. Seitsonen, A. Smogunov, I. Timrov, T. Thonhauser, P. Umari, N. Vast, X. Wu, S. Baroni, Advanced capabilities for materials modelling with Quantum ESPRESSO, Journal of Physics: Condensed Matter. 29 (2017) 465901. https://doi.org/10.1088/1361-648X/aa8f79.

[23] J.P. Perdew, K. Burke, M. Ernzerhof, Generalized Gradient Approximation Made Simple, Phys Rev Lett. 77 (1996) 3865–3868. https://doi.org/10.1103/PhysRevLett.77.3865.

[24] H.J. Monkhorst, J.D. Pack, Special points for Brillouin-zone integrations, Phys Rev B. 13 (1976) 5188–5192. https://doi.org/10.1103/PhysRevB.13.5188.

[25] D.P. Woodruff, D. Brown, P.D. Quinn, T.C.Q. Noakes, P. Bailey, Structure determination of surface adsorption and surface alloy phases using medium energy ion scattering, Nucl Instrum Methods Phys Res B. 183 (2001) 128–139. https://doi.org/10.1016/S0168-583X(01)00472-4.

[26] L.J. Clarke, L. Morales De La Garza, Chlorine superstructures on Mo(110) investigated by LEED and AES, Surface Science Letters. 121 (1982) A362. https://doi.org/10.1016/0167-2584(82)90635-1.

[27] N.G. Hörmann, A. Grossa, P. Kaghazchi, Semiconductor-metal transition induced by nanoscale stabilization, Physical Chemistry Chemical Physics. 17 (2015) 5569–5573. https://doi.org/10.1039/c4cp05619a.

Figure Captions

Fig. 1. (a) Structure and basis vectors, $\boldsymbol{a}_i, \boldsymbol{a}_i', \boldsymbol{a}_i''(i = 1,2)$ of Mo(110). The (3×1) is specified relative to $\boldsymbol{a}_i'$, and the (1×3) and (1×4) are relative to $\boldsymbol{a}_i''$. Note that $\boldsymbol{a}_i$ defines diffraction indices for 1×1 clean surface and all *I-V* curves in Fig. 3 since diffraction spots intensity for LEED analysis were recorded individually from sets of symmetrically equivalent beams. "1" − "5" sites denote the substitutional and overlayer sites of a single Sn atom, respectively. (b) – (e) LEED patterns for clean (1×1), Sn induced (3×1), (1×3), (1×4) surfaces with reciprocal lattice vectors, $\boldsymbol{b}_i, \boldsymbol{b}_i', \boldsymbol{b}_i''(i = 1,2)$. All the LEED patterns were taken at an incident electron energy of 195 eV.

Fig. 2. Top and side views of determined structure models for (a) 3×1, (b) 1×3, and (c) 1×4. S1-S4 denote positions of Sn, while M1 – M4 of Mo. In (b) and (c), the size of Sn atom is reduced to show the adsorption site clearly. The red dashed circles in (b) with a radius of ~3.3 Å and (c) with a radius of ~3.2 Å are guides for atomic distances nearby and coordination numbers. Refer to Tables 2 - 4 for detailed structure parameters.

Fig. 3. Comparison of experimental (black) and theoretical (red) LEED *I-V* curves for (a) 3×1, (b) 1×3 and (c) 1×4. Note that the spot indices are defined by the primitive lattice vectors, $\boldsymbol{a}_1$, $\boldsymbol{a}_2$ shown in Fig. 1(a).

Tables

Table.1 Calculated adsorption energies of single Sn atoms.

No.	Adsorption site	E_{ads} (eV/atom)
1	Substitutional	-4.61
2	Four-fold hollow	-4.22
3	Three-fold hollow	-4.05
4	Short bridge	-3.84
5	On-top	-3.46

Table.2 Atomic positions and their errors for the optimized (3×1) structure determined by LEED analysis. Also listed are the parameters obtained by DFT. All the units are in Å. Refer to the model in Fig. 2(a) for the symbols and atoms. Mo atoms in the second layer (Mo3~5) are shifted by $\sim\frac{1}{2}\boldsymbol{a_1''}$ relative to those in the first layer.

Symbol	Atom	LEED					DFT		
		[001]		$[1\bar{1}0]$	[110]		[001]	$[1\bar{1}0]$	[110]
S1	Sn1	0.00*		0.00*	0.56	±0.02	0.00*	0.00*	0.65
M1	Mo1	3.11	±0.03	0.00*	0.00	±0.01	3.06	0.00*	0.00
M2	Mo2	6.32	±0.03	0.00*	0.00	±0.01	6.38	0.00*	0.00
M3	Mo3	1.57	±0.03	0.00*	-2.11	±0.01	1.58	0.00*	-2.11
M4	Mo4	4.72*		0.00*	-2.11	±0.02	4.72*	0.00*	-2.06
M5	Mo5	7.87	±0.03	0.00*	-2.11	±0.01	7.86	0.00*	-2.11

* denotes that the position is fixed due to symmetry.

Table. 3 Atomic positions and their errors for the optimized (1×3) structure determined by LEED analysis. Also listed are the parameters obtained by DFT. All the units are in Å. Refer to the model in Fig. 2(b) for the symbols and atoms. Mo atoms in the second layer (Mo4~6) are shifted by $\sim\frac{1}{2}\boldsymbol{a_1''}$ relative to those in the first layer.

Symbol	Atom		LEED					DFT	
		[001]	$[1\bar{1}0]$		[110]		[001]	$[1\bar{1}0]$	[110]
S1	Sn1	3.15*	1.85	±0.09	2.37	±0.07	3.15	1.69	2.44
S2	Sn1	4.72*	5.14	±0.15	2.37	±0.05	4.75	5.03	2.43
M1	Mo1	0.00*	0.00	±0.12	0.00	±0.03	0.00	0.00	0.00
M2	Mo2	1.57*	2.39	±0.09	-0.15	±0.06	1.57	2.23	0.00
M3	Mo3	3.15*	4.70	±0.09	-0.10	±0.03	3.15	4.43	-0.01
M4	Mo4	1.57*	0.00	±0.12	-2.30	±0.03	1.57	0.00	-2.24
M5	Mo5	3.15*	2.11	±0.13	-2.31	±0.04	3.15	2.22	-2.24
M6	Mo6	4.72*	4.41	±0.03	-2.30	±0.03	4.72	4.43	-2.22

* denotes that the position is fixed due to symmetry.

Table 4. Atomic positions and their errors for the optimized (1×4) structure determined by LEED analysis. Also listed are the parameters obtained by DFT. All the units are in Å. Refer to the model in Fig. 2(c) for the symbols and atoms. Mo atoms in the second layer (Mo5~8) are shifted by $\sim\frac{1}{2}\boldsymbol{a_1''}$ relative to those in the first layer.

Symbol	Atom	LEED					DFT		
		[001]	[1$\bar{1}$0]		[110]		[001]	[1$\bar{1}$0]	[110]
S1	Sn1	1.57*	0.00*		2.44	±0.03	1.57	0.00	2.50
S2	Sn2	3.15*	2.91	±0.06	2.40	±0.02	3.15	2.88	2.44
S3	Sn3	3.15*	5.99	±0.06	2.40	±0.02	3.15	6.02	2.44
M1	Mo1	0.00*	0.00*		0.00	±0.03	0.00	0.00	0.00
M2	Mo2	1.57*	2.23	±0.05	-0.01	±0.02	1.57	2.22	0.00
M3	Mo3	3.15*	4.45*		-0.02	±0.03	3.15	4.45	-0.02
M4	Mo4	4.72*	6.68	±0.05	0.00	±0.02	4.72	6.68	0.00
M5	Mo5	1.57*	0.00*		-2.22	±0.02	1.57	0.00	-2.21
M6	Mo6	3.15*	2.23	±0.07	-2.22	±0.02	3.15	2.21	-2.20
M7	Mo7	4.72*	4.45*		-2.22	±0.02	4.72	4.45	-2.18
M8	Mo8	6.29*	6.68	±0.07	-2.22	±0.02	6.29	6.70	-2.20

* denotes that the position is fixed due to symmetry.

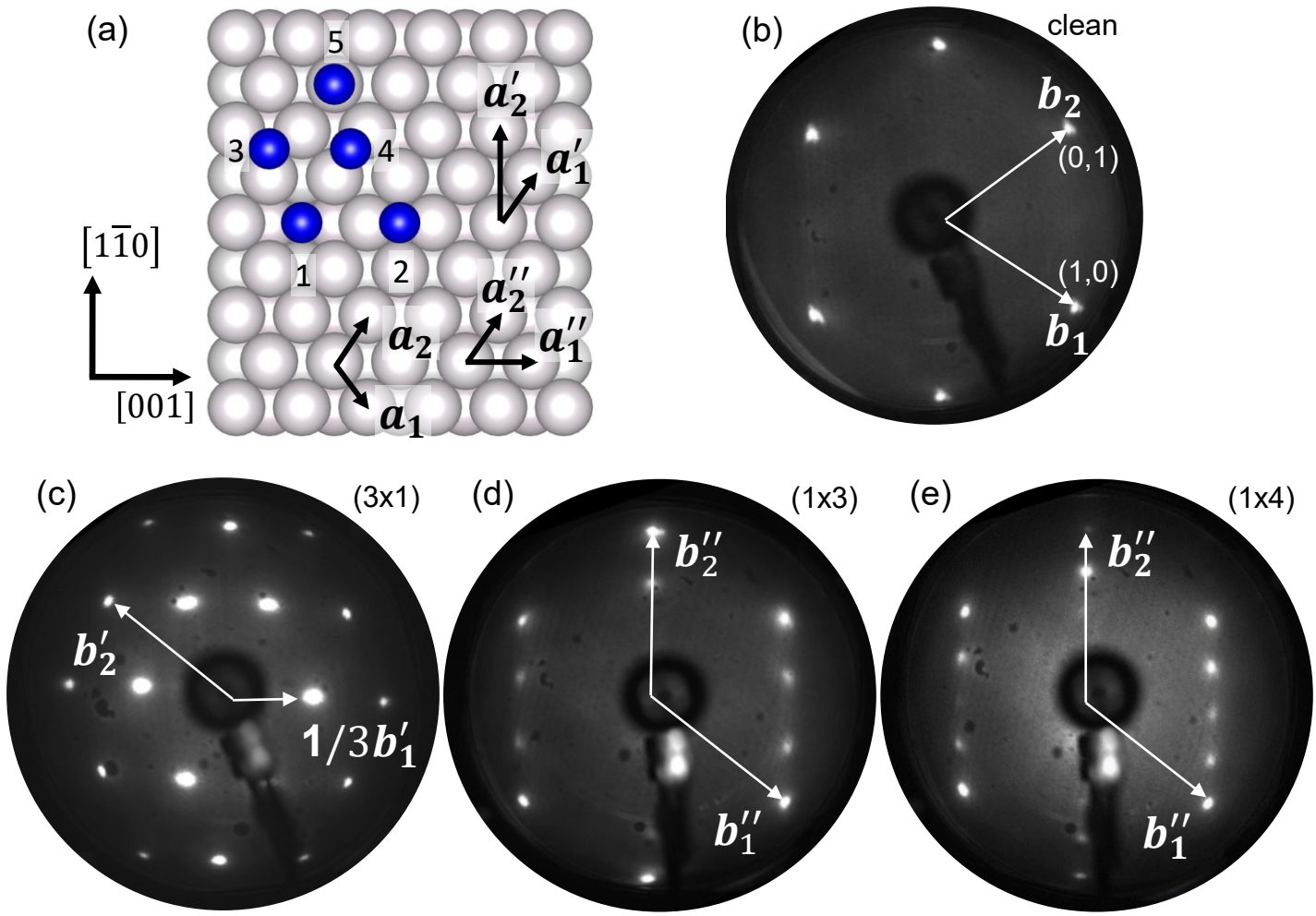
(a)
5
3
4
1
2
$[1\bar{1}0]$
$[001]$
a_2'
a_1'
a_2''
a_1''
a_2
a_1
(b)
clean
b_2
(0,1)
(1,0)
b_1
(c)
(3x1)
b_2'
$1/3b_1'$
(d)
(1x3)
b_2''
b_1''
(e)
(1x4)
b_2''
b_1''

Fig.1

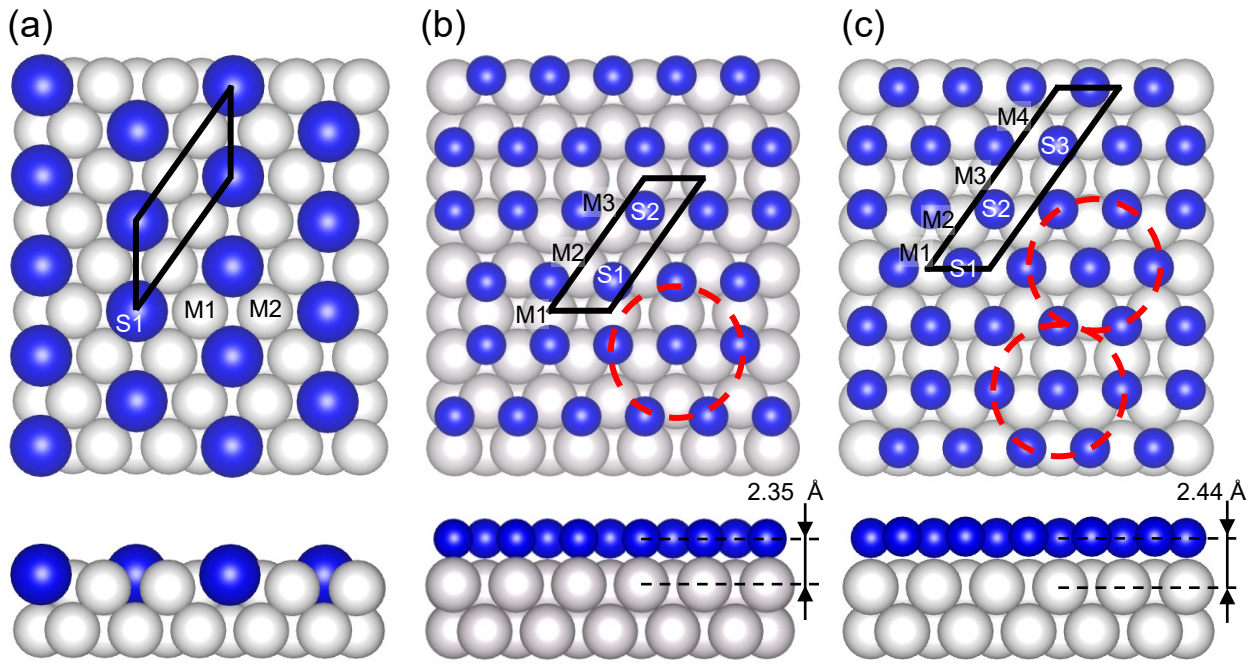

Fig.2

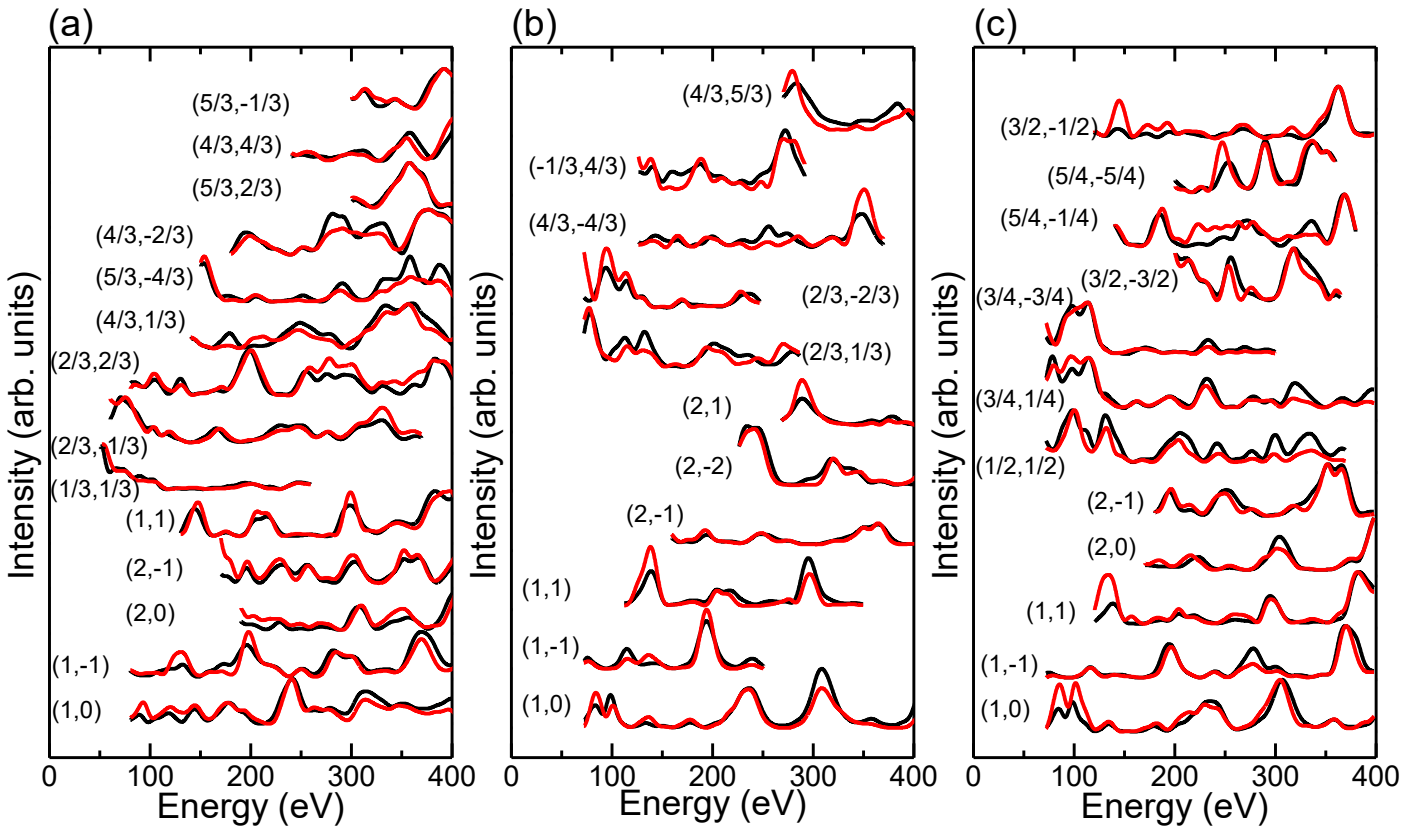
(a)
(5/3,-1/3)
(4/3,4/3)
(5/3,2/3)
(4/3,-2/3)
(5/3,-4/3)
(4/3,1/3)
(2/3,2/3)
(2/3,1/3)
(1/3,1/3)
(1,1)
(2,-1)
(2,0)
(1,-1)
(1,0)
Intensity (arb. units)
0
100
200
300
400
Energy (eV)
(b)
(4/3,5/3)
(-1/3,4/3)
(4/3,-4/3)
(2/3,-2/3)
(2/3,1/3)
(2,1)
(2,-2)
(2,-1)
(1,1)
(1,-1)
(1,0)
Intensity (arb. units)
0
100
200
300
400
Energy (eV)
(c)
(3/2,-1/2)
(5/4,-5/4)
(5/4,-1/4)
(3/2,-3/2)
(3/4,-3/4)
(3/4,1/4)
(1/2,1/2)
(2,-1)
(2,0)
(1,1)
(1,-1)
(1,0)
Intensity (arb. units)
0
100
200
300
400
Energy (eV)

Fig.3

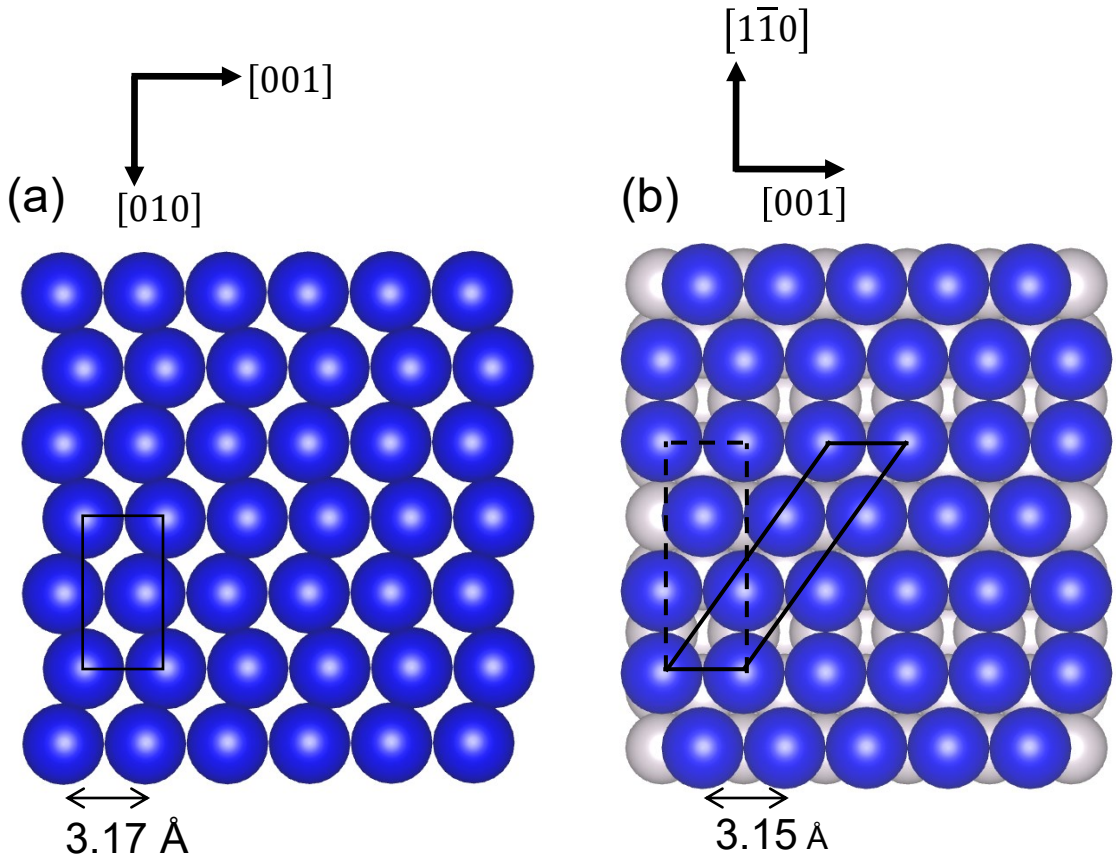

Fig.S1